ACS Photonics

Article

Cite This: ACS Photonics XXXX, XXX, XXX−XXX

pubs.acs.org/journal/apchd5

Tuning Topology of Photonic Systems with Transparent Conducting Oxides

Zhaxylyk A. Kudyshev,* Alexander V. Kildishev,* Alexandra Boltasseva, and Vladimir M. Shalaev

School of Electrical and Computer Engineering and Birck Nanotechnology Center, Purdue University, West Lafayette, Indiana 47907, United States

Supporting Information

ABSTRACT: Precise control over photonic states can be achieved in pre-engineered materials, like photonic crystals and meta-structures. However, high fabrication precisions are required due to the sensitivity of such states to different perturbation channels. Hence photonic states that immune to disorder in the system is in high demand. In this work, we propose a hybrid platform that integrates tunable transparent conducting oxides (TCOs) and a standard silicon-on-insulator waveguide technology, to achieve ultrafast all-optical control of the topology of photonic states. Particularly, we demonstrate that ultrafast control of coupling between ring resonators with integrated TCO modulators enables a synthetic gauge magnetic field and therefore provides ultrafast control of topology protection. The approach can be used for the realization of topological phase transitions, an essential component of several emerging photonic applications, including topologically protected optical modulators and switches.

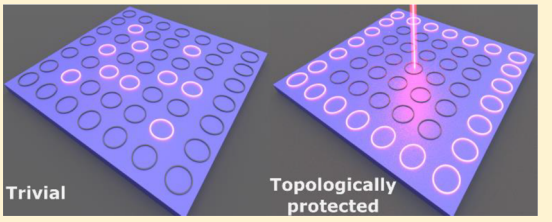

KEYWORDS: *tunable photonic topological insulators, ultrafast topology control, gauge magnetic field control, transparent conducting oxides*

Symmetry is a fundamental concept that defines physical effects in many areas. Different types of symmetry breaking lead to the realization of various exotic phenomena, such as the formation of topologically protected states in Fermionic systems.[1,2] Recently it has been demonstrated that the concept of topological protection can be extended to bosonic systems as well, which opened a way for the realization of a conceptually new class of photonic platforms, photonic topological insulators.[3−6] The field of topological photonics attracted significant interest in the community due to its importance for both understanding fundamental light−matter interaction and the realization of advanced photonic applications.[7,8] Photonic devices utilizing topological protection could substantially increase the robustness of the photonic modes for different perturbations. Such protection has been theoretically predicted and experimentally demonstrated within diverse photonic platforms in the broadband spectral range.[9−13] Photonic topological insulators have been realized based on a different variation of meta-structures, such as metamaterials with a strong gyrotropic response and all-dielectric 3D metamaterials.[14−16] Different types of photonic crystals with pre-engineered band-structure have been used for the realization of photonic topological insulators.[17,18] Along with the aforementioned approaches, topologically protected states for photons are realized in the system of coupled ring resonators. It has been demonstrated that specific arrangement of the coupling between resonators in the system leads to the generation of a synthetic magnetic field for photons in the system and realization of robust edge photonic states.[19−26] Recently it has been demonstrated that photonic topological insulators can be used for lasing,[27−30] different quantum applications,[31,32] and unidirectional guiding.[31]

The development and advancements of new material platforms offer new avenues of light−matter interaction control. Recent investigations of optically and electrically tunable transparent conducting oxides (TCOs), for example, indium−tin oxide (ITO) and aluminum-doped zinc oxide (AZO), combined with the progress in the materials' fabrication techniques, make TCOs a promising platform for on-chip photonics.[33,34] TCO's optical properties can be tailored/adjusted via various means, for example, either by altering the stoichiometry, deposition conditions, or through annealing.[35,36] Hence, a lightly doped TCO enables dielectric optical response in the near-infrared wavelength range with a refractive index close to that of glass, while a highly doped TCO can be used as a plasmonic material.[37] Most importantly, TCOs extreme dynamic modulation of their optical properties can be obtained via either electrical or optical excitation.[38,38−43]

Within this work, we show that integrating TCOs with silicon-on-insulator (SOI) technology provides ultrafast optical/electrical tunning of the synthetic gauge magnetic field and enables dynamic topology control of photonic systems.

Received: September 27, 2018
Published: July 29, 2019

DOI: 10.1021/acsphotonics.8b01355
ACS Photonics XXXX, XXX, XXX−XXX

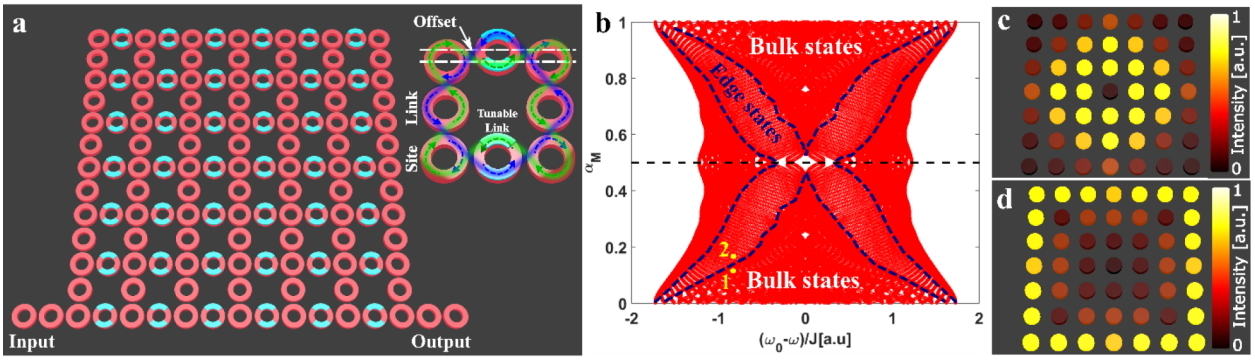

Figure 1. (a) Schematics of the AZO-controlled integrated array of coupled SOI ring resonators (a unit cell and the corresponding spin-up (blue) and spin-down (green) traces are shown in the inset). (b) Hofstadter butterfly spectrum for a 7 × 7 resonator system. The boundary between topologically trivial and topologically protected edge state bands of interest is outlined by the dashed curve. The horizontal dashed line corresponds to $\alpha_M = \frac{1}{2}$. (c, d) Mode distributions, which correspond to a topologically trivial bulk state (outlined on (b) as (1)) and topologically protected edge state (outlined on (b) as (2)), respectively. Topologically protected edge states (d) are locked to the edge of the device and are insensitive to geometric perturbation of the system and protected against scattering from defects. In contrast, topologically trivial bulk states (c) are sensitive to all perturbation channels mentioned above.

TIGHT-BINDING MODEL

One way to realize topologically protected states in a photonic system proposed in refs 21, 44, and 45 is to use an array of coupled ring resonators (Figure 1a). Inset in Figure 1a shows a unit cell of the structure, which consists of four "site" resonators and four "link" couplers. The "link" waveguides have a slightly different length in comparison with "site" resonators, which makes them detuned from resonant condition to ensure energy confinement in the "site" resonators. The "site" rings are coupled only to their neighboring "link" waveguides. Following the notation introduced in ref 21, the clockwise propagating modes inside the unit cell are denoted as spin-up states, while anticlockwise propagating modes with spin-down states (see Figure 1a, inset, where spin-ups are highlighted in blue and spin-downs are shown in green). To enable degeneracy of the two spin states, two different propagation phases should be accumulated for the modes hoping in the forward and backward directions. Such phase difference is achieved with shifting one of the "link" waveguides from its symmetry position in the unit cell by a vertical offset of ξ (inset in Figure 1a). The offset leads to the difference in the optical path for spin-up and spin-down states, which in turn gives a desired accumulated phase $\phi = 2\pi\alpha_M = 4\pi n_{mod}\xi/\lambda$, where n_{mod} is a modal index and λ is a wavelength of light. The Hamiltonian of such system can be described by the Harper-Hofstadter model:[46]

$$H_0 = \sum_{x,y} \hat{b}^{\dagger}_{x,y}\hat{b}_{x,y} - J\left(\sum_{x,y} \hat{b}^{\dagger}_{x+1,y}\hat{b}_{x,y}e^{-iy\phi} + \hat{b}^{\dagger}_{x,y}\hat{b}_{x+1,y}e^{iy\phi} + \hat{b}^{\dagger}_{x,y+1}\hat{b}_{x,y} + \hat{b}^{\dagger}_{x,y}\hat{b}_{x,y+1}\right) \quad (1)$$

where $\hat{b}^{\dagger}_{x,y}$ ($\hat{b}_{x,y}$) is the creation (annihilation) operator at the site (x, y) and J is the effective tunneling rate between resonators. Since the behavior of such a system is identical to the dynamics of charged particles in a uniform external magnetic field, it supports quantum Hall effect for photons. Figure 1b shows the Hofstadter butterfly spectrum, eigenvalues of the Hamiltonian plotted as a function of the applied magnetic field. The ratio $\alpha_M = p/q$ determines the band structure of the system; here, p and q are prime numbers. In this case, the system has q allowed bands (populated with nontopologically protected bulk states) and $q - 1$ band-gaps. In the case of the finite-sized structure, band-gaps are filled with topologically protected edge-states. The boundaries between topologically nonprotected bulk and topologically protected edge state bands of interest are outlined by the dashed curve. However, there are several band-gaps populated by the protected edge states not outlined here.[46]

Precise control of the synthetic gauge magnetic field can be realized by controlling the mode index of the "link" waveguides. By choosing the working wavelength and proper design of waveguide array, it is possible to realize a photonic state that lays in the vicinity of the forbidden band gap, such that change of "link" waveguide mode index will transfer topologically nonprotected bulk to the topologically protected-edge states and vice versa, that is, make transition between the states (1) and (2) in Figure 1b. Figure 1c,d shows the mode distributions, which correspond to bulk state (1) and topologically protected edge state (2), respectively.

ULTRAFAST CONTROL OF SYNTHETIC MAGNETIC FIELD WITH TCOS

To achieve ultrafast control of a gauge magnetic field, we propose to use a silicon resonator array on silicon dioxide integrated with an AZO layer as a dynamically tunable material. Previously it has been demonstrated that modulation of the TCO's optical response can be achieved via optical pumping.[47−49] The pump with an energy greater than the band gap is used to move valence band electrons up into the conduction band. The excited electrons, in turn, alter the properties of the material until the electrons and holes recombine. This method generates free carriers throughout the bulk of the entire film (≈100 nm) and is only limited by the material absorption (≈10 fs) and recombination time. It has also been shown that up to 500% relative changes in the AZO linear refractive index can be achieved.[47] In ref 48, ultrafast and large intensity-dependent linear refractive index responses in an ITO film around the ENZ point, with an index modulation of 170% and a recovery time of about 360 fs was demonstrated.

Here we assume that AZO films have a 3% dopant concentration, which results in a crossover frequency of 0.55

DOI: 10.1021/acsphotonics.8b01355
ACS Photonics XXXX, XXX, XXX−XXX

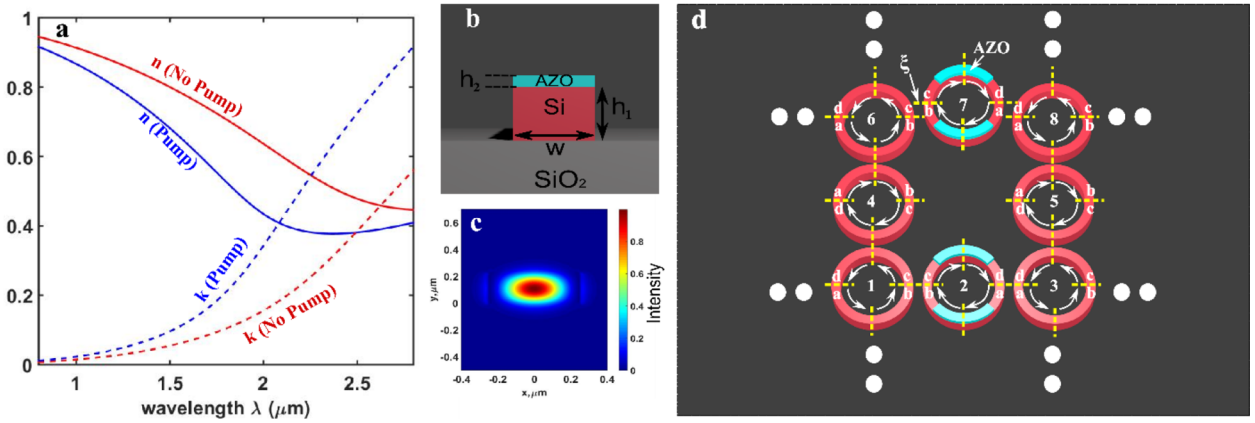

Figure 2. (a) Real (solid) and imaginary (dashed) parts of the refractive index of the AZO film at two regimes without pump (No Pump, red) and with pump (Pump, blue). (b) Cross-section of the AZO integrated tunable "link" waveguide: on a silicon dioxide substrate. (c) Fundamental mode distribution inside tunable link waveguide. (d) The unit cell used within transfer matrix formalism for strongly coupled microring resonators. Each ring is divided into four sections; the junctions between sections are shown with the dashed yellow lines.

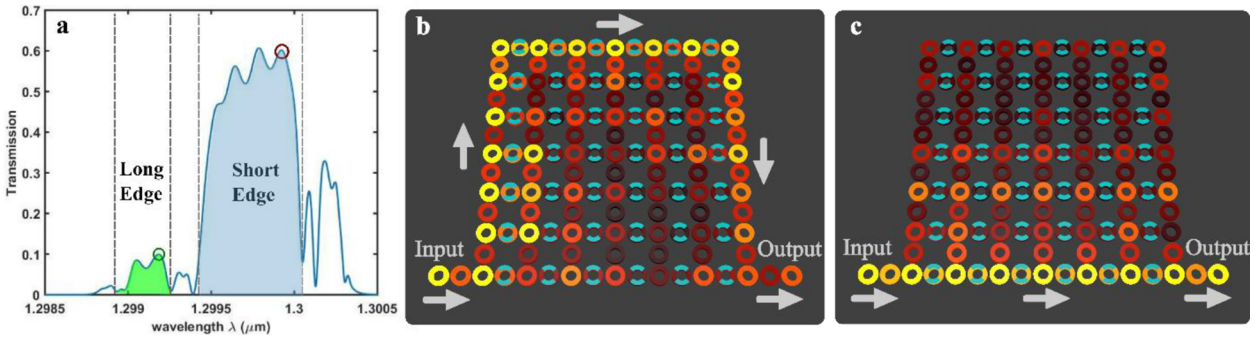

Figure 3. (a) Transmission spectrum of the 7 × 7 photonic lattice without pump: two highlighted regions correspond to short (blue) and long (green) topologically protected edge state bands; (b, c) field distributions for the topologically protected modes: long-edge (b) and short-edge (c) modes. Corresponding wavelengths are marked in (a) by green and red circles at 1.2992 and 1.2998 μm, respectively.

eV (frequency at which $\mathcal{R}(\varepsilon(\omega))$ crosses zero) and a damping coefficient of 0.2 eV. Therefore, the refractive index of AZO film at 1.3 μm is equal to $n_{AZO}^{unpump} = 0.8506 + i0.034$.[34,36] Additionally, we assume that optical pumping introduces 10% change of the real part of the refractive index at 1.3 μm and results in $n_{AZO}^{pump} = 0.766 + i0.0567$. The dispersion of AZO film is shown in Figure 2a. Dispersion dynamics is determined based on the assumption of achievable 16% modulation of crossover frequency by optical pumping of TCOs.[34]

To realize ultrafast control over the mode index of link waveguides, we propose to partially cover tunable "link" waveguides with a 50 nm thin AZO layer. Cross-section of such a tunable link waveguide is shown in Figure 2b. Here we assume that all resonators have 510 × 220 nm^2 cross-section that ensures single-mode propagation in the near-infrared spectral range. Without loss of generality, we are focusing on the 1.3 μm working wavelength; however, by modifying the geometry of the resonators as well as AZO doping level, it is possible to shift the working wavelength at the telecom frequency band of 1.5 μm.

To determine mode indexes of the fundamental mode in the tunable "link" waveguide in unpumped and pumped regimes, we have performed mode analysis using Lumerical MODE Solutions. Fundamental mode distribution inside tunable link waveguide is shown in Figure 2c. In the unpumped regime, the mode index of the tunable link waveguide is $n_{mod}^{unpump} = 2.7030 + i0.0019$, while in pumped regime the mode index becomes $n_{mod}^{pump} = 2.7016 + i0.0022$. We note that it is demonstrated that more complex designs of TCO modulators[38,50] could provide an even stronger change of the mode index, hence, enabling higher tunability of gauge magnetic field, as well as a smaller attenuation.

RESULTS

Here we use a transfer matrix method, adapted from ref 51. The unit cell used within transfer matrix formalism for strongly coupled microring resonators is shown on Figure 2d. Each ring is divided into four sections; the junctions between sections are shown with the dashed yellow lines. More details of the transfer matrix approach are provided in the Supporting Information. We considered an AZO-integrated tunable photonic system, built on an array of 7 × 7 site microring resonators (see Figure 1a). We have determined transmission and coupling coefficients of the system by using variational finite-difference time domain analysis of an add/drop filter and the system of two "site" resonators coupled via "link" coupler (Lumerical MODE Solutions). The total length, $L_{SR} = 65$ μm, of the "site" resonators provides a resonant response around 1.3 μm, while the length of the "link" waveguide is detuned from the resonant condition by $\eta = 150$ nm ($L_{LR} = 65.15$ μm). The 100 nm gaps between ring resonators and 12.8 μm coupling length make the effective coupling coefficient κ_{ij} =

DOI: 10.1021/acsphotonics.8b01355
ACS Photonics XXXX, XXX, XXX−XXX

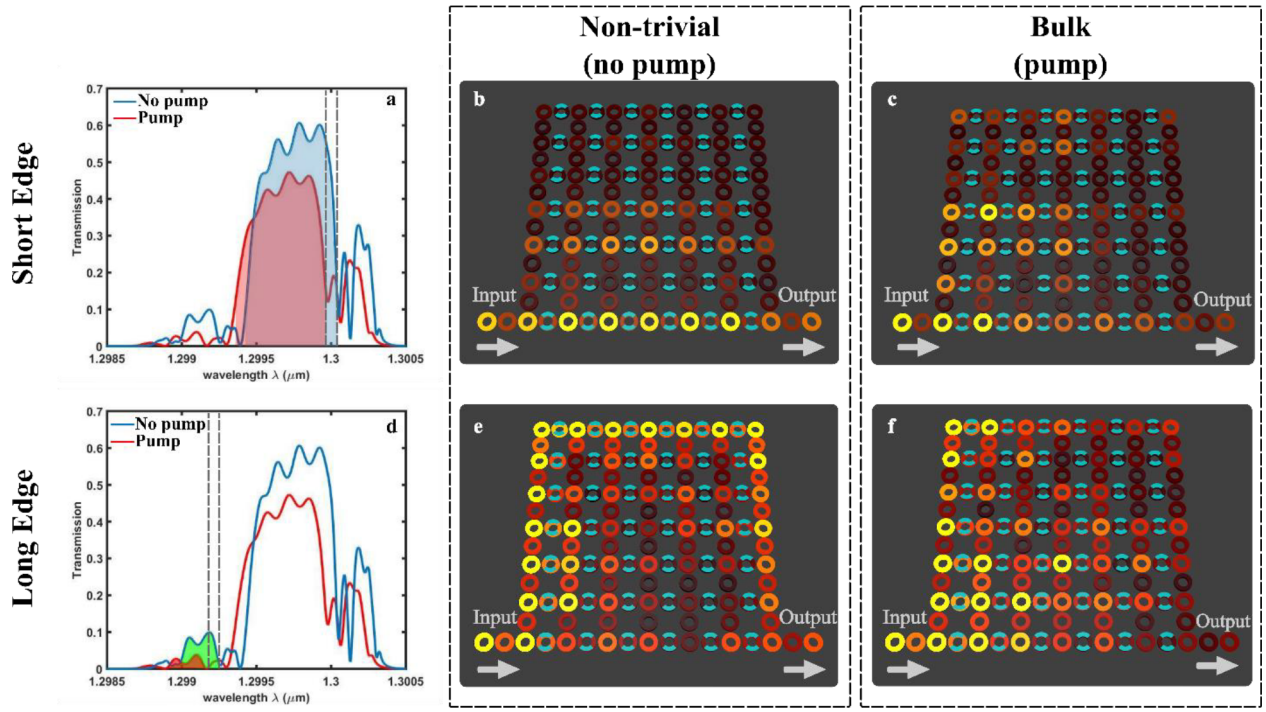

Figure 4. (a, d) Transmission spectra of the 7 × 7 photonic lattice without (blue) and with (red) pump (a) "Short-edge" topologically protected bands without (blue highlight) and with (red highlight) pump. Modulation gap between topologically trivial and protected state bands is indicated by dashed lines. (b, c) Field distribution inside the photonic lattice without (b) and with (c) pump at 1.3 μm. (d) "Long-edge" topologically protected bands without (green highlight) and with (red highlight) pump. (e, f) Field distributions inside the photonic lattice without (e) and with (f) pump for the "long-edge" band.

0.41, while a 120 nm gap with the input/output couplers assures κ_{in} = 0.48. The AZO layer covers 30% of the link couplers and does not overlap with the coupling regions to achieve uniform coupling throughout the sample (see the inset in Figure 1a).

TUNABLE PROTECTION OF PHOTONIC STATES

Displacement of the tunable link waveguides by ζ = 90 nm makes α_M = 0.1883 and, in general, creates six topologically protected bands around a 1.3 μm wavelength. For further discussion, we focus on the outermost two bands in the Hofstadter spectrum (shown in Figure 1). Figure 3a shows the transmission spectrum of the 7 × 7 photonic system for the unpumped regime when the effective mode index of the AZO-covered tunable link waveguide becomes n_{mod}^{unpump}. The two highlighted regions (Figure 3a) correspond to short and long topologically protected edge state bands. The boundaries between topologically protected and trivial states are outlined with dashed lines. Short-edge states correspond to spin-down states (counterclockwise propagating modes), while long-edge states are referred to as spin-up states (clockwise propagating modes) based on the path length they travel through the lattice from input to the output. Figure 3b shows the long-edge mode distribution inside the lattice, which corresponds to the wavelength marked by a green circle in Figure 3a.

Figure 3c shows the energy distribution of the topologically protected short-edge mode (wavelength is marked in Figure 3a by a red circle). Arrows indicate propagation directions of the mode inside the lattice. Dimensions of the microring resonators array are chosen such that the mode at a wavelength of 1.3 μm lies on the edge of the topologically protected band (short-edge) for the unpumped regime. In the pumped regime, the effective mode index of the AZO covered part of the tunable "link" waveguides is switched from n_{mod}^{unpump} to n_{mod}^{pump}, thus, blue-shifting the transmission spectrum in comparison with the unpumped case. As a result, the mode corresponding to 1.3 μm becomes topologically nonprotected under the pump illumination.

Figure 4a shows the transmission spectra of light propagating through the photonic system in the unpumped (blue line) and pumped (red line) regimes. Dashed lines indicate the available modulation gap between topologically nonprotected and protected state bands. Figure 4b,c shows the field distribution inside the photonic lattice in the unpumped (b) and pumped (c) regimes at a wavelength of 1.3 μm. Due to the aforementioned transition of the system, transmission through photonic lattice changes from 47% (topologically protected) to 16% (topologically nonprotected). As seen from these dependencies, the optical control of the AZO photonic lattice changes the topological protection of a photonic state at the desired wavelength range. It is possible to achieve a transition between the long-edge protected and the topologically nonprotected states as well. Long-edge topologically protected bands in the unpumped and pumped cases are represented in Figure 4d by green and red shadowing, respectively. Dashed lines indicate the modulation gap between the topologically nonprotected and protected state bands. Here, we note that the modulation of the AZO optical properties leads to a "long-edge"−"bulk" state transition around 1.299 μm. The mode distributions of the "long-edge" state (unpumped) and bulk state (pump) are shown in Figure 4e,f. Because of such a transition, the transmission through the photonic lattice becomes less than 1% for the topologically trivial (pumped regime), while it is 9% for the "long-edge"

DOI: 10.1021/acsphotonics.8b01355
ACS Photonics XXXX, XXX, XXX−XXX

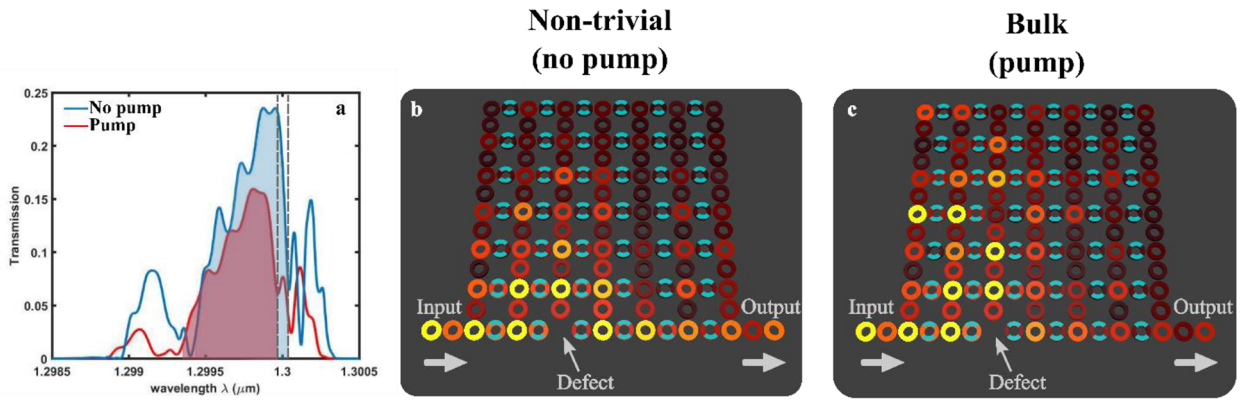

Figure 5. (a) Transmission spectra of the 7 × 7 photonic lattice with a defect (missing resonator) along the edge for unpumped and pumped regimes. (b) Field distribution of the topologically protected "short-edge" mode (unpumped regime) and bulk mode (pumped regime) at 1.3 μm in the case of the photonic lattice with a single defect.

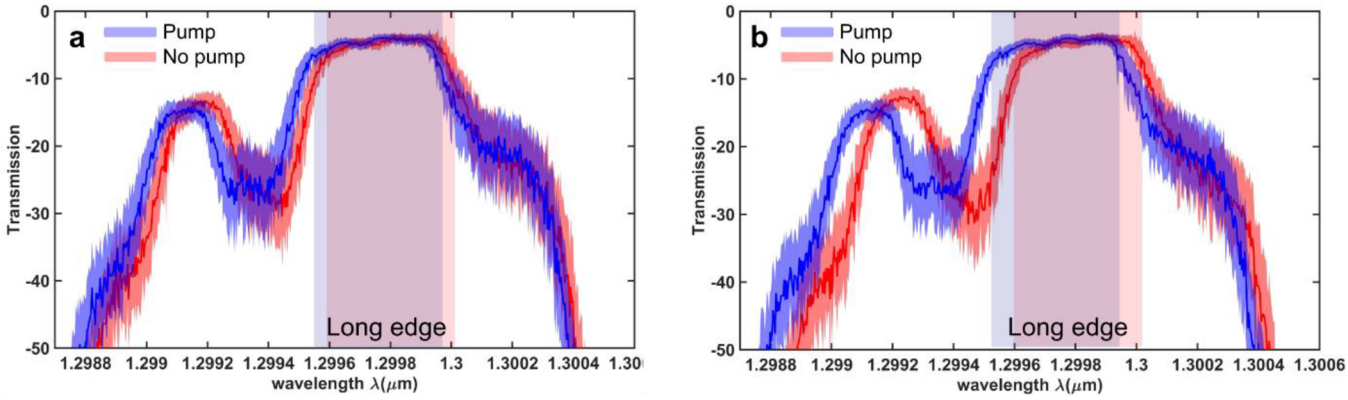

Figure 6. Transmission spectrum of a lattice in the presence of disorders for unpumped and pumped cases for two different modulation levels of the AZO junction: (a) 2.5% and (b) 5%. The solid curves correspond to mean values of the spectra, while the shaded regions correspond to the standard deviation resulting from disorder. Averaging is performed over 100 different realizations for each of the cases.

state. By choosing the right dimensions of the microring resonator array, it is possible to achieve "long-edge" topology modulation at the desired wavelength. Here, we optimized our system to have the desired modulation for "short-edge" state at 1.3 μm.

To demonstrate the robustness of the topologically protected states, the case of the photonic lattice with a missing resonator along one of the sides of the sample is considered (Figure 5b,c). Here, we chose short-edge topologically protected state at 1.3 μm. We would expect that due to the topological robustness the edge state (unpumped regime) would bypass the impurity without scattering into bulk, while the trivial bulk mode (pumped regime) would lead to the reduction of the transmission due to scattering on such defect. Transmission spectra of the 7 × 7 resonator system with the defect for unpumped and pumped regimes are shown in Figure 5a. In the case of the topologically protected mode (unpumped case) at 1.3 μm, the transmission is 19%, in comparison with 7% at the pumped case, topologically nonprotected mode. Field distributions of the topologically protected and non-protected, trivial modes are shown in Figure 5b and c, respectively. As expected, the topologically protected edge state bypasses the defect and does not acquire additional scattering losses, while in the pumped regime, the mode is topologically nonprotected and scatters into the bulk.

Here we would like to underline the effect of photonic losses.[52] The above analysis indicates that the overall transmission through topologically protected channels is below 100%. The main reason for this is the propagation losses in the tunable waveguide couplers introduced by the AZO modulator junctions. A possible way of solving this issue is to use either more advanced high-efficiency modulator designs or to optimize TCO material composition that would provide the same order of tunability at a lower attenuation level. High-efficiency modulator designs can be obtained based on conventional optimization techniques or by using inverse design optimization methods, such as topology optimization[53] and machine learning assisted inverse design optimization.[54] The optical properties of TCOs can be efficiently adjusted via doping and tuning the fabrication parameters,[55,56] providing an additional degree of freedom for designing highly efficient, low-loss modulators. For example, AZO permittivity is strongly dependent on oxygen pressures upon deposition. Tuning the pressure level[56] can be used to optimize optical properties at the wavelength band of interest. Another tuning option is to carefully adjust the dopant level of AZO, which could enable a significant reduction of ohmic losses in the band of interest. More details are provided in the Supporting Information. To sum up, a careful adjustment of material properties (material composition and deposition condition), as well as overall

DOI: 10.1021/acsphotonics.8b01355
ACS Photonics XXXX, XXX, XXX−XXX

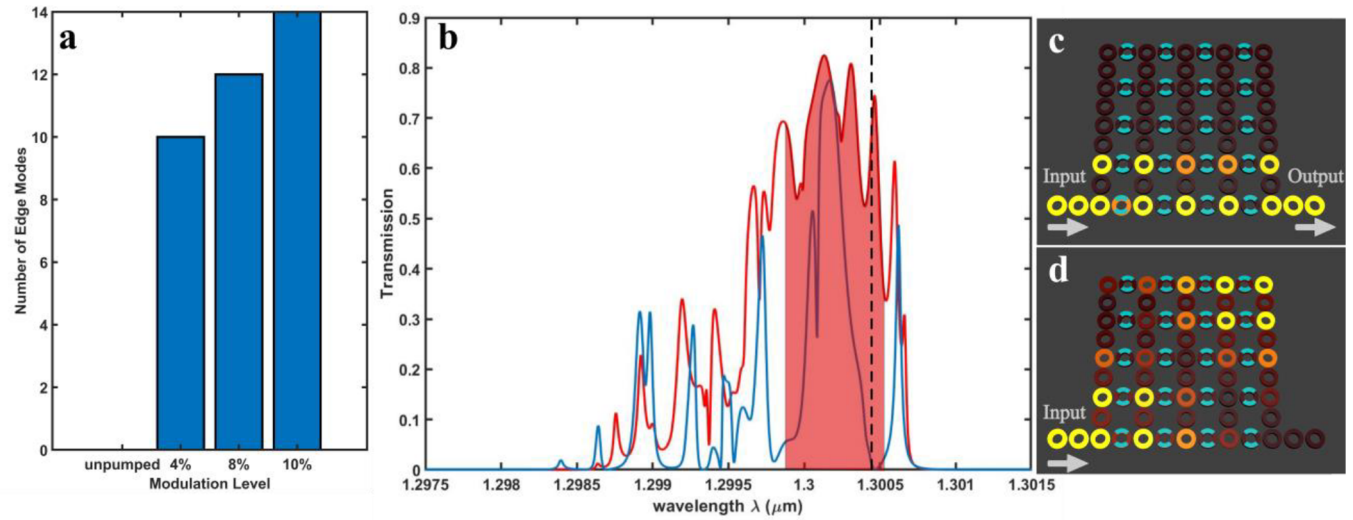

Figure 7. (a) The number of topologically protected modes in the system under different modulation levels. (b) Transmission spectra of the 5 × 5 photonic lattice for unpumped (blue) and 10% modulation level case (red). (c, d) Field distributions of the topologically protected mode (10% modulation) and the topologically trivial mode (unpumped regime) at 1.3004 μm (shown with a dashed vertical line on (b)).

microring resonators array configuration, should enable a significant reduction of the signal attenuation in the system.

Another important issue is the robustness of the approach against fabrication imperfections. Due to limited fabrication tolerance, device realization is associated with different perturbations of the key system parameters, such as mismatch of the ring resonance frequencies, variations in the coupling constant and the loss rate. Particularly, we consider the case when the total length of each resonator (L_{SR}) and each coupler (L_{LR}) has a ±10 nm random deviation from the standard uniform distribution, while the coupling between the waveguides has a 4% random mismatch from the ideal value defined by $\tilde{\kappa}_{ij} = \kappa_{ij} + 0.04\kappa_{ij}\delta$, here κ_{ij} is an ideal coupling coefficient, δ-random number generated from the standard uniform distribution.

We have considered a 7 × 7 photonic system where each resonator and the coupling junction have a random perturbation outlined above. Figure 6 shows the transmittance spectrum of a lattice in the presence of disorders for unpumped and pumped cases. The solid curves correspond to mean values of the spectra, while the shaded region corresponds to the standard deviation resulting from the disorder. Averaging is performed over 100 different realizations for each of the cases. We have assumed 2.5% and 5% modulation of the tunable AZO junctions. The figure indicates that the edge state regions are significantly less affected by the introduced perturbations, that is, their transmittance is least affected, while bulk-state regions are significantly affected by the noise. This result is in total agreement with the experimental verification done in ref 45. By pumping the system, it is possible to obtain the spectral modulation gaps between the protected photon state and the bulk state. However, due to disorder, not all of the realization produces the desired switch between the states. The analysis of the field distribution inside the 7 × 7 resonator system at 1.3 μm resonant wavelength reveals that 39 out of 100 realization leads to the topologically protected edge and nonprotected bulk-states switch in the case of 2.5% modulation. In the case of 5% modulation of the AZO junction, 61 realization leads to the topologically protected edge state to nonprotected bulk state transformation out of 100.

TOPOLOGICAL PHASE TRANSITION

The proposed approach can be extended to enable a phase transition between different states of a photonic topological system. As outlined above, the state of a photonic topological insulator is determined by an applied synthetic gauge magnetic field α_M and can be mapped into Hofstadter butterfly via $\alpha_M = p/q$, the ratio that defines the number of bands and forbidden gaps. To realize a topological phase transition, one could utilize the fact that the center-most bands are degenerate at the gauge fields which correspond to even q values.[46] This condition can be satisfied by optimizing the proposed TCO microring resonator array, thus, enabling a topological insulator with a closed central band gap. The topological phase transition is achieved by modulation of the synthetic magnetic field, which leads to the formation of new bands with different Chern numbers. One interesting case can be realized using $\alpha_M = 1/2$ the gauge field configuration (shown by the black dashed line in Figure 1b), which corresponds to the case of the trivial state of two bands connected via Dirac point.[57] A perturbation of the gauge field might lead to reopening of the central gap, hence transferring the system to a nontrivial topological state. For example, by tuning the gauge field from $\alpha_M = 0.5$ ($p = 1$, $q = 2$) to $\alpha_M = 0.4$ ($p = 2$, $q = 5$), it is possible to transfer the system from a trivial configuration to a topologically nontrivial state with five bands and to correspond four band-gaps filled with topologically protected states for a finite-size lattice.

To demonstrate this effect, we consider a photonic system with AZO-integrated 5 × 5 microring resonators. Displacement of the tunable link waveguides by $\zeta = 715$ nm makes $\alpha_M = 0.5$ ($p = 1$, $q = 2$) and brings the system into the trivial state with no topologically protected edge modes. The synthetic gauge magnetic field is tuned by pumping the tunable link waveguides to achieve $\alpha_M = 0.545$ ($p = 109$, $q = 200$), which brings the system into a nontrivial topological state. The advanced band structure calculations can be used for detailed analysis of such cases.[57] Here, we assume that the AZO based modulator covers 30% of tunable link waveguides and enables up to 10% modulation of the modal index. To verify this, we determined the number of topologically protected edge modes in the system under different modulation level: unpumped, 4%,

DOI: 10.1021/acsphotonics.8b01355
ACS Photonics XXXX, XXX, XXX−XXX

8%, and 10% modulation of AZO coupled junctions of tunable link waveguide (Figure 7a). As expected, topologically protected states vanish in the unpumped regime which corresponds to a photonic state with trivial topology, while in the pumped case there are several detectable topologically protected edge modes in the system. The number of topologically protected states is increasing with the increasing modulation level. This effect can be explained by the fact that a higher modulation level corresponds to a higher synthetic magnetic field and leads to wider band gaps. The transmission spectra of trivial (unpumped) and nontrivial (10% modulation of tunable link waveguides) states are shown in Figure 7b, where a clear formation of the transmission plateau, corresponding to a topologically protected band highlighted by the red shadowing, is depicted. The dashed vertical line indicates the frequency corresponding to the two field distributions inside the system for the nontrivial (Figure 7c) and trivial (Figure 7d) cases. Thus, we demonstrate that the proposed method enables the topology phase transformation of the photonic states from trivial to nontrivial regimes.

One of the possible applications of the topological phase transition is high-efficiency, backscattering-free optical modulators. Along with the high-order modulation of transmission (see Figure 7b), the topological transformation ensures the robustness of the device to the external perturbations and makes a modulated signal immune to backscattering due to its topological protection. A critical remaining question that requires a more detailed analysis is related to the minimal achievable footprint of the modulator built on the topological phase transition. Since topological protection is a property of the entire system, there should be a minimum for the number of unit cells that could support such protection.

SUMMARY AND OUTLOOK

In this work, we theoretically demonstrate that exploiting dynamic properties of transparent conducting oxides in combination with silicon on insulator technology provides a pathway to ultrafast, all-optical control over the topology of photonic states. We consider an array of strongly coupled ring resonators supporting the photonic quantum Hall effect due to a pre-engineered synthetic magnetic field. We demonstrate that, by integrating the aforementioned photonic system with Al-doped ZnO-based modulators, it is possible to control the magnetic field by optical pumping precisely; similar control can be realized via electrical gating as well. By choosing the operating wavelength and proper design of the waveguide array, one can realize a photonic state that lays in the vicinity of the forbidden bandgap, such that modulation of the synthetic magnetic field induces the transition between the topologically protected edge state and the topologically nonprotected bulk photonic state. Moreover, spatiotemporal modulation of the gating or pumping could enable advanced, ultrafast control over topologically protected photonic modes both in space and in time. Ultrafast control of the topological states of a photonic system opens up new frontiers in photonics, condensed matter physics, and quantum optics and could lead to significant advances in the fundamental science of light−matter interaction as well as in subwavelength light control for practical on-chip devices with picosecond switching rates.

ASSOCIATED CONTENT

Supporting Information

The Supporting Information is available free of charge on the ACS Publications website at DOI: 10.1021/acsphotonics.8b01355.

Loss issue and comparison between different doping levels of AZO film in modulator junction and the transfer matrix method for the coupled waveguide system (PDF)

AUTHOR INFORMATION

Corresponding Authors

*E-mail: zkudyshev@purdue.edu.

*E-mail: kildishev@purdue.edu.

ORCID

Zhaxylyk A. Kudyshev: 0000-0002-6955-0890

Notes

The authors declare no competing financial interest.

ACKNOWLEDGMENTS

This work was supported in part by the U.S. Department of Energy (DE-SC0017717; A.B.), NSF (0939370-CCF; Z.K.), DARPA/DSO Extreme Optics and Imaging (EXTREME) Program (HR00111720032; A.K.), and ONR (N00014-18-1-2481; V.S.).

REFERENCES

(1) Hsieh, D.; Qian, D.; Wray, L.; Xia, Y.; Hor, Y. S.; Cava, R. J.; Hasan, M. Z. A Topological Dirac Insulator in a Quantum Spin Hall Phase. *Nature* **2008**, *452* (7190), 970−974.

(2) Xia, Y.; Qian, D.; Hsieh, D.; Wray, L.; Pal, A.; Lin, H.; Bansil, A.; Grauer, D.; Hor, Y. S.; Cava, R. J.; et al. Observation of a Large-Gap Topological-Insulator Class with a Single Dirac Cone on the Surface. *Nat. Phys.* **2009**, *5* (6), 398−402.

(3) Haldane, F. D. M.; Raghu, S. Possible Realization of Directional Optical Waveguides in Photonic Crystals with Broken Time-Reversal Symmetry. *Phys. Rev. Lett.* **2008**, *100* (1), No. 013904.

(4) Raghu, S.; Haldane, F. D. M. Analogs of Quantum-Hall-Effect Edge States in Photonic Crystals. *Phys. Rev. A: At., Mol., Opt. Phys.* **2008**, *78* (3), No. 033834.

(5) Weimann, S.; Kremer, M.; Plotnik, Y.; Lumer, Y.; Nolte, S.; Makris, K. G.; Segev, M.; Rechtsman, M. C.; Szameit, A. Topologically Protected Bound States in Photonic Parity−time-Symmetric Crystals. *Nat. Mater.* **2017**, *16*, 433−438.

(6) Gao, F.; Gao, Z.; Shi, X.; Yang, Z.; Lin, X.; Xu, H.; Joannopoulos, J. D.; Soljačić, M.; Chen, H.; Lu, L.; Chong, Y.; Zhang, B. Probing Topological Protection Using a Designer Surface Plasmon Structure. *Nat. Commun.* **2016**, *7* (1), 11619.

(7) Lu, L.; Joannopoulos, J. D.; Soljačić, M. Topological Photonics. *Nat. Photonics* **2014**, *8* (11), 821−829.

(8) Khanikaev, A. B.; Shvets, G. Two-Dimensional Topological Photonics. *Nat. Photonics* **2017**, *11*, 763−773.

(9) Noh, J.; Huang, S.; Chen, K. P.; Rechtsman, M. C. Observation of Photonic Topological Valley Hall Edge States. *Phys. Rev. Lett.* **2018**, *120* (6), No. 063902.

(10) Lu, L.; Joannopoulos, J. D.; Soljačić, M. Topological States in Photonic Systems. *Nat. Phys.* **2016**, *12*, 626−629.

(11) Shalaev, M. I.; Desnavi, S.; Walasik, W.; Litchinitser, N. M. Reconfigurable Topological Photonic Crystal. *New J. Phys.* **2018**, *20* (2), No. 023040.

(12) Cheng, X.; Jouvaud, C.; Ni, X.; Mousavi, S. H.; Genack, A. Z.; Khanikaev, A. B. Robust Reconfigurable Electromagnetic Pathways within a Photonic Topological Insulator. *Nat. Mater.* **2016**, *15* (5), 542−548.

DOI: 10.1021/acsphotonics.8b01355
ACS Photonics XXXX, XXX, XXX−XXX

(13) Zhou, H.; Peng, C.; Yoon, Y.; Hsu, C. W.; Nelson, K. A.; Fu, L.; Joannopoulos, J. D.; Soljacic, M.; Zhen, B. Observation of Bulk Fermi Arc and Polarization Half Charge from Paired Exceptional Points. *Science* **2018**, *359* (6379), 1009−1012.
(14) Khanikaev, A. B.; Mousavi, S. H.; Tse, W. K.; Kargarian, M.; MacDonald, A. H.; Shvets, G. Photonic Topological Insulators. *Nat. Mater.* **2013**, *12* (3), 233−239.
(15) Ma, T.; Khanikaev, A. B.; Mousavi, S. H.; Shvets, G. Guiding Electromagnetic Waves around Sharp Corners: Topologically Protected Photonic Transport in Metawaveguides. *Phys. Rev. Lett.* **2015**, *114* (12), 127401.
(16) Gao, W.; Lawrence, M.; Yang, B.; Liu, F.; Fang, F.; Béri, B.; Li, J.; Zhang, S. Topological Photonic Phase in Chiral Hyperbolic Metamaterials. *Phys. Rev. Lett.* **2015**, *114* (3), No. 037402.
(17) Barik, S.; Miyake, H.; DeGottardi, W.; Waks, E.; Hafezi, M. Two-Dimensionally Confined Topological Edge States in Photonic Crystals. *New J. Phys.* **2016**, *18* (11), 113013.
(18) Wu, L. H.; Hu, X. Scheme for Achieving a Topological Photonic Crystal by Using Dielectric Material. *Phys. Rev. Lett.* **2015**, *114* (22), 223901.
(19) Fang, K.; Yu, Z.; Fan, S. Realizing Effective Magnetic Field for Photons by Controlling the Phase of Dynamic Modulation. *Nat. Photonics* **2012**, *6* (11), 782−787.
(20) Hafezi, M.; Lukin, M. D.; Taylor, J. M. Non-Equilibrium Fractional Quantum Hall State of Light. *New J. Phys.* **2013**, *15* (6), No. 063001.
(21) Hafezi, M.; Mittal, S.; Fan, J.; Migdall, A.; Taylor, J. M. Imaging Topological Edge States in Silicon Photonics. *Nat. Photonics* **2013**, *7* (12), 1001−1005.
(22) Blanco-Redondo, A.; Andonegui, I.; Collins, M. J.; Harari, G.; Lumer, Y.; Rechtsman, M. C.; Eggleton, B. J.; Segev, M. Topological Optical Waveguiding in Silicon and the Transition between Topological and Trivial Defect States. *Phys. Rev. Lett.* **2016**, *116* (16), 163901.
(23) Plotnik, Y.; Bandres, M. A.; Stützer, S.; Lumer, Y.; Rechtsman, M. C.; Szameit, A.; Segev, M. Analogue of Rashba Pseudo-Spin-Orbit Coupling in Photonic Lattices by Gauge Field Engineering. *Phys. Rev. B: Condens. Matter Mater. Phys.* **2016**, *94* (2), No. 020301.
(24) Bandres, M. A.; Rechtsman, M. C.; Segev, M. Topological Photonic Quasicrystals: Fractal Topological Spectrum and Protected Transport. *Phys. Rev. X* **2016**, *6* (1), No. 011016.
(25) Rechtsman, M. C.; Plotnik, Y.; Zeuner, J. M.; Song, D.; Chen, Z.; Szameit, A.; Segev, M. Topological Creation and Destruction of Edge States in Photonic Graphene. *Phys. Rev. Lett.* **2013**, *111* (10), 103901.
(26) Rechtsman, M. C.; Zeuner, J. M.; Plotnik, Y.; Lumer, Y.; Podolsky, D.; Dreisow, F.; Nolte, S.; Segev, M.; Szameit, A. Photonic Floquet Topological Insulators. *Nature* **2013**, *496* (7444), 196−200.
(27) Bandres, M. A.; Wittek, S.; Harari, G.; Parto, M.; Ren, J.; Segev, M.; Christodoulides, D. N.; Khajavikhan, M. Topological Insulator Laser: Experiments. *Science* **2018**, *359* (6381), eaar4005.
(28) Harari, G.; Bandres, M. A.; Lumer, Y.; Rechtsman, M. C.; Chong, Y. D.; Khajavikhan, M.; Christodoulides, D. N.; Segev, M. Topological Insulator Laser: Theory. *Science* **2018**, *359* (6381), eaar4003.
(29) Zhao, H.; Miao, P.; Teimourpour, M. H.; Malzard, S.; El-Ganainy, R.; Schomerus, H.; Feng, L. Topological Hybrid Silicon Microlasers. *Nat. Commun.* **2018**, *9* (1), 981.
(30) Bahari, B.; Ndao, A.; Vallini, F.; El Amili, A.; Fainman, Y.; Kanté, B. Nonreciprocal Lasing in Topological Cavities of Arbitrary Geometries. *Science* **2017**, *358* (6363), 636−640.
(31) Perczel, J.; Borregaard, J.; Chang, D. E.; Pichler, H.; Yelin, S. F.; Zoller, P.; Lukin, M. D. Topological Quantum Optics in Two-Dimensional Atomic Arrays. *Phys. Rev. Lett.* **2017**, *119* (2), No. 023603.
(32) Barik, S.; Karasahin, A.; Flower, C.; Cai, T.; Miyake, H.; DeGottardi, W.; Hafezi, M.; Waks, E. A Topological Quantum Optics Interface. *Science* **2018**, *359* (6376), 666−668.
(33) Kinsey, N.; DeVault, C.; Kim, J.; Ferrera, M.; Shalaev, V. M.; Boltasseva, A. Epsilon-near-Zero Al-Doped ZnO for Ultrafast Switching at Telecom Wavelengths. *Optica* **2015**, *2* (7), 616.
(34) Kim, J.; Carnemolla, E. G.; DeVault, C.; Shaltout, A. M.; Faccio, D.; Shalaev, V. M.; Kildishev, A. V.; Ferrera, M.; Boltasseva, A. Dynamic Control of Nanocavities with Tunable Metal Oxides. *Nano Lett.* **2018**, *18* (2), 740−746.
(35) Kim, J.; Naik, G. V.; Emani, N. K.; Guler, U.; Boltasseva, A. Plasmonic Resonances in Nanostructured Transparent Conducting Oxide Films. *IEEE J. Sel. Top. Quantum Electron.* **2013**, *19* (3), 4601907−4601907.
(36) Naik, G. V.; Kim, J.; Boltasseva, A. Oxides and Nitrides as Alternative Plasmonic Materials in the Optical Range [Invited]. *Opt. Mater. Express* **2011**, *1* (6), 1090.
(37) Naik, G. V.; Shalaev, V. M.; Boltasseva, A. Alternative Plasmonic Materials: Beyond Gold and Silver. *Adv. Mater.* **2013**, *25*, 3264−3294.
(38) Babicheva, V. E.; Kinsey, N.; Naik, G. V.; Ferrera, M.; Lavrinenko, A. V.; Shalaev, V. M.; Boltasseva, A. Towards CMOS-Compatible Nanophotonics: Ultra-Compact Modulators Using Alternative Plasmonic Materials. *Opt. Express* **2013**, *21* (22), 27326.
(39) Cai, W.; White, J. S.; Brongersma, M. L. Compact, High-Speed and Power-Efficient Electrooptic Plasmonic Modulators. *Nano Lett.* **2009**, *9* (12), 4403−4411.
(40) Feigenbaum, E.; Diest, K.; Atwater, H. A. Unity-Order Index Change in Transparent Conducting Oxides at Visible Frequencies. *Nano Lett.* **2010**, *10* (6), 2111−2116.
(41) Abb, M.; Sepúlveda, B.; Chong, H. M. H.; Muskens, O. L. Transparent Conducting Oxides for Active Hybrid Metamaterial Devices. *J. Opt.* **2012**, *14* (11), 114007.
(42) Abb, M.; Albella, P.; Aizpurua, J.; Muskens, O. L. All-Optical Control of a Single Plasmonic Nanoantenna - ITO Hybrid. *Nano Lett.* **2011**, *11* (6), 2457−2463.
(43) Traviss, D.; Bruck, R.; Mills, B.; Abb, M.; Muskens, O. L. Ultrafast Plasmonics Using Transparent Conductive Oxide Hybrids in the Epsilon-near-Zero Regime. *Appl. Phys. Lett.* **2013**, *102* (12), 121112.
(44) Mittal, S.; Fan, J.; Faez, S.; Migdall, A.; Taylor, J. M.; Hafezi, M. Topologically Robust Transport of Photons in a Synthetic Gauge Field. *Phys. Rev. Lett.* **2014**, *113* (8), No. 087403.
(45) Mittal, S.; Ganeshan, S.; Fan, J.; Vaezi, A.; Hafezi, M. Measurement of Topological Invariants in a 2D Photonic System. *Nat. Photonics* **2016**, *10* (3), 180−183.
(46) Hofstadter, D. R. Energy Levels and Wave Functions of Bloch Electrons in Rational and Irrational Magnetic Fields. *Phys. Rev. B* **1976**, *14* (6), 2239−2249.
(47) Caspani, L.; Kaipurath, R. P. M.; Clerici, M.; Ferrera, M.; Roger, T.; Kim, J.; Kinsey, N.; Pietrzyk, M.; Di Falco, A.; Shalaev, V. M.; Boltasseva, A.; Faccio, D. Enhanced Nonlinear Refractive Index in ϵ -Near-Zero Materials. *Phys. Rev. Lett.* **2016**, *116* (23), 1−5.
(48) Alam, M. Z.; De Leon, I.; Boyd, R. W. Large Optical Nonlinearity of Indium Tin Oxide in Its Epsilon-near-Zero Region. *Science* **2016**, *352* (6287), 795−797.
(49) Hommelhoff, P.; Kling, M. F.; Stockman, M. I. Ultrafast Phenomena on the Nanoscale. *Ann. Phys.* **2013**, *525* (1−2), A13−A14.
(50) Babicheva, V. E.; Boltasseva, A.; Lavrinenko, A. V. Transparent Conducting Oxides for Electro-Optical Plasmonic Modulators. *Nanophotonics* **2015**, *4*, 165−185.
(51) Tsay, A.; Van, V. Analytic Theory of Strongly-Coupled Microring Resonators. *IEEE J. Quantum Electron.* **2011**, *47* (7), 997−1005.
(52) Hafezi, M.; Demler, E. A.; Lukin, M. D.; Taylor, J. M. Robust Optical Delay Lines with Topological Protection. *Nat. Phys.* **2011**, *7* (11), 907−912.
(53) Molesky, S.; Lin, Z.; Piggott, A. Y.; Jin, W.; Vucković, J.; Rodriguez, A. W. Inverse Design in Nanophotonics. *Nat. Photonics* **2018**, *12* (11), 659−670.

DOI: 10.1021/acsphotonics.8b01355
ACS Photonics XXXX, XXX, XXX−XXX

(54) Bor, E.; Alparslan, O.; Turduev, M.; Hanay, Y. S.; Kurt, H.; Arakawa, S.; Murata, M. Integrated Silicon Photonic Device Design by Attractor Selection Mechanism Based on Artificial Neural Networks: Optical Coupler and Asymmetric Light Transmitter. *Opt. Express* **2018**, *26* (22), 29032.
(55) Boltasseva, A.; Atwater, H. A. Low-Loss Plasmonic Metamaterials. *Science* **2011**, *331*, 290−291.
(56) Kim, H.; Osofsky, M.; Prokes, S. M.; Glembocki, O. J.; Piqué, A. Optimization of Al-Doped ZnO Films for Low Loss Plasmonic Materials at Telecommunication Wavelengths. *Appl. Phys. Lett.* **2013**, *102* (17), 171103.
(57) Harper, F.; Simon, S. H.; Roy, R. Perturbative Approach to Flat Chern Bands in the Hofstadter Model. *Phys. Rev. B: Condens. Matter Mater. Phys.* **2014**, *90* (7), No. 075104.

DOI: 10.1021/acsphotonics.8b01355
ACS Photonics XXXX, XXX, XXX−XXX